Biosensors and Bioelectronics 143 (2019) 111561

Contents lists available at ScienceDirect

Biosensors and Bioelectronics

journal homepage: www.elsevier.com/locate/bios

An organic electrochemical transistor integrated with a molecularly selective isoporous membrane for amyloid-β detection

Shofarul Wustoni[a], Shaofei Wang[a,b], Juan R. Alvarez[a,b], Tania C. Hidalgo[a], Suzana P. Nunes[a,b], Sahika Inal[a,*]

[a] Biological and Environmental Science and Engineering, King Abdullah University of Science and Technology (KAUST), Thuwal, 23955-6900, Saudi Arabia
[b] Advanced Membranes and Porous Materials Center, KAUST, Thuwal, 23955-6900, Saudi Arabia

ARTICLE INFO

Keywords:
Organic electrochemical transistor
Bioelectronics
Nanoporous membrane
Biosensor
Amyloid-β

ABSTRACT

Alzheimer's disease (AD) is a progressive neurodegenerative disease associated with severe memory loss and impaired cognitive skills. A common pathological change found in AD-affected brains is the accumulation of a peptide named amyloid-β (Aβ) that can form plaques. Aβ aggregates are visible to structural scanning tools; however, these bulky and expensive instruments are accessible to trained personnel in clinical settings only, thus hampering timely diagnosis of the disease, particularly in low-resource settings. In this work, we design an organic electrochemical transistor (OECT) for *in vitro* detection of Aβ aggregates in human serum. The OECT channel is integrated with a nanostructured isoporous membrane which has a strong affinity for Aβ aggregates. The detection mechanism relies on the membrane capturing Aβ aggregates larger than the size of its pores and thus blocking the penetration of electrolyte ions into the channel underneath. Combining the high transconductance of the OECT with the precise porosity and selectivity of the membrane, the device detects the presence of Aβ aggregates in human serum samples with excellent sensitivity. This is the first-time demonstration of a biofunctionalized, nanostructured, and isoporous membrane integrated with a high-performance transistor for biosensing. This robust, low-power, non-invasive, and miniaturized sensor aids in the development of point-of-care tools for early diagnosis of AD.

1. Introduction

Alzheimer's disease (AD) is a neurodegenerative disorder that impairs memory and cognitive functions with a progressive decline of physical and mental fitness. In 2018, more than 45 million people worldwide are estimated to be living with the disease, accounting for an economic cost over 600 billion USD annually due to prolonged care as well as productivity loses (Vas et al., 2001). Alzheimer's Disease International, a nonprofit organization, forecasted the number of people diagnosed with AD to triple to ca. 150 million by 2050 (Alzheimer's Disease International, 2018). While there are currently no treatments to stop AD from progressing, early diagnosis is crucial to help the patient to adjust to the symptoms, and benefit from available treatments that can slow down the irreversible damage to healthy cells.

It is now well accepted that the peptide amyloid-β (Aβ) plays a role in the development of AD (LaFerla et al., 2007). From its regular, short-chain polypeptide state (i.e., "the monomer", ca. 40–42 residues in length), Aβ can assemble into various aggregated forms known as oligomers, protofibrils (soluble, elongated aggregates) and fibrils (Hardy and Selkoe, 2002). In its monomeric state, Aβ is not neurotoxic; however, the aggregates of Aβ accumulate gradually into plaques in specific regions of the brain. These plaques are believed to be responsible for blocking communication between neurons, leading to neuronal loss, which is the hallmark of AD (Walsh et al., 2002). Currently, the diagnosis of AD is not straightforward and relies mainly on cognitive tests combined with methods that screen for these neurotoxic assemblies of Aβ in the brain or cerebrospinal fluid. To monitor Aβ aggregates and quantify their concentration, fluorescence methods have been commonly utilized (Dalal et al., 2012; Pinotsi et al., 2013). While neuroimaging techniques are expensive and require sophisticated instrumentation and a clinical setting, biochemical assays lack sensitivity and require tedious preparation steps, expensive labels and operation time. A simple, rapid and inexpensive tool for *in vitro* detection of Aβ aggregates is imperative, especially in low-income countries where access to such instrumentation and assays is limited. For a progressive disease like AD, early diagnosis is essential in order to slow down the damage with the right treatment.

Electrochemical techniques have been proposed as a label-free

* Corresponding author.
E-mail address: sahika.inal@kaust.edu.sa (S. Inal).

https://doi.org/10.1016/j.bios.2019.111561
Received 10 May 2019; Received in revised form 21 July 2019; Accepted 31 July 2019
Available online 05 August 2019
0956-5663/

alternative for the detection of Aβ aggregation (Vestergaard et al., 2005; Liu et al., 2014). In most cases, the detection relies on the oxidation of the redox active residue in the Aβ primary structure (i.e., tyrosine (Tyr)) by an electrode in its vicinity (Lopes et al., 2014; Suprun et al., 2016). However, the aggregation of the protein affects the proximity of Tyr to the transducing electrode; thus, the oxidation signal weakens during the monomer-to-fibril transition. Also, this detection scheme suffers from poor selectivity because of the nonspecific adsorption of peptides onto the electrode surface and electrochemical interference from other electroactive groups in the Aβ backbone (e.g. methionine and histidine) or in the measurement solution (Schöneich et al., 2003). Despite the simplicity of electrochemical detection, these methods have thus largely remained complementary to optical techniques.

Among electrochemical transducing elements, organic electrochemical transistors (OECTs) show exceptional performance for biochemical sensing (Pappa et al., 2018; Wang et al., 2019). An OECT is a three terminal device comprising of a channel made of an ion-permeable organic electronic material in direct contact with the measurement solution (electrolyte) into which a gate electrode is immersed (Rivnay et al., 2018). The device translates small ionic fluxes in the electrolyte into a large electrical readout from the channel. The identifying characteristic of an OECT is the injection barrier-free penetration of electrolyte ions into the bulk of the organic channel, causing a large modulation of the carrier density therein. The transducing event is thus coupled with amplification, and endows the OECT with high gain at low voltages (< 1 V). For the detection of a particular species, the OECT channel or the gate electrode should be functionalized with a bio-recognition element such as nucleotides or proteins. Via such functionalization routes, OECTs could detect pH changes (Mariani et al., 2018), metal cations (Ghittorelli et al., 2018), metabolites (Wustoni et al., 2019), neurotransmitters (Gualandi et al., 2016), pathogens (He et al., 2012) and antibodies (Macchia et al., 2018), as well as disease-specific antigens and proteins (Kim et al., 2010). Due to the non-redox nature of antibody-antigen (Ab-Ag) interactions, development of immunosensors based on OECTs has been more challenging and thus, sparse (Kim et al., 2010; Macchia et al., 2018; Fu et al., 2017). Although most of the sensors have excellent sensitivity due to the gain of the OECT and the strong and specific interactions between Ag and Ab, the biochemical modification of micron-scale surfaces lacks the desired precision, and are highly complex and cost ineffective. Moreover, the integration of biomolecules with two-dimensional surfaces can result in loss or change of their function. The immobilization of recognition units is also known to lead to degradation of the electronic material underneath, compromising the intrinsic gain of the transistor. In addition, with such biological coating on the surfaces, the devices are typically for single-use, despite the cost.

One strategy to mitigate these issues without compromising on sensitivity and selectivity is to interpose a separate film for molecular recognition between the channel and the gate of an OECT (Sessolo et al., 2014; Parlak et al., 2018). As the detection layer and the device are physically separated, the electronic components are no longer chemically modified to anchor biorecognition units and the design of both the device and the sensing layer can be less stringent. Here, we demonstrate a molecularly functionalized, nanostructured, and isoporous membrane and its integration with a high gain, ion-to-electron transducing device, the OECT. Our nanostructured isoporous membrane has a pore size smaller than 50 nm and a surface functionalized with Congo red, i.e., a ligand with a strong affinity to a cross-β structure of Aβ aggregates. We integrate this membrane with a microscale OECT by interposing it vertically, in between the channel and the electrolyte. As the membrane selectively captures Aβ aggregates in solution, the proteins become immobilized on its surface. With a size larger than that of the membrane pores, the Aβ aggregates block the transport of ions from the electrolyte into the channel, suppressing the gating of the OECT. The OECT signal thus varies depending on the concentration of Aβ aggregates in the solution. Our approach will open up a new avenue for the design of electronic immunosensors and aid in the development of low-cost, portable, stable and high-performance electronic tools for early diagnosis of progressive diseases such as AD.

2. Experimental methods

2.1. Materials

We purchased the block copolymer poly(styrene-*b*-4-vinylpyridine) (P10900-S4VP, 188000-*b*-64000 g/mol) from Polymer Source, Inc., Canada. Dimethylformamide, 1,4-dioxane, acetone, 4-chloro-1-butanol, ethanol (EtOH), (3-aminopropyl)triethoxysilane (APTES), glutaraldehyde (GA), Congo red (CR), ethylene glycol (EG), dodecyl benzene sulfonic acid (DBSA), (3-glycidyloxypropyl)trimethoxysilane (GOPS), potassium ferricyanide ($K_3Fe(CN)_6$), ammonium hydroxide, human serum from human male AB plasma and phosphate buffered saline (PBS) were purchased from Sigma-Aldrich. We purchased the conducting polymer poly(ethylenedioxythiophene):poly(styrenesulfonate) (PEDOT:PSS, PH1000) dispersion from Heraeus Clevios GmbH, the recombinant human amyloid β 1–42 peptide (#ab82795) from Abcam (Cambridge, MA, USA), and glass beads from Polysciences, Inc. We prepared all aqueous solutions with ultrapure water (Milli-Q, Millipore).

2.2. Functionalization of the nanoporous membrane

We prepared the pristine nanoporous membrane from the block copolymer poly(styrene-*b*-4-vinylpyridine), PS-*b*-P4VP, according to a previously published procedure (Madhavan et al., 2014). This process is known as self-assembly and non-solvent-induced phase separation of block copolymers and described in Figure S1. To covalently attach the recognition units on the membrane surface, the first step involved the quaternization of the 4VP block using 4-chlorobutan-1-ol. We immersed the membrane in a 2.5% (v/v) solution of 4-chlorobutan-1-ol in ethanol in a beaker at room temperature for 24 h. The membrane was taken out and washed with water. We then exposed the quaternized membranes to a 5% (v/v) solution of (3-aminopropyl)triethoxysilane (APTES) in water for 30 minutes, followed by rinsing with ultrapure water. The next step was the immobilization of Congo red molecules on the quaternized membrane using glutaraldehyde (GA) as the crosslinker. We immersed the amine-terminated membranes in 5% (w/v) GA solution for 30 min and then rinsed with PBS and dried with N_2 spray. Congo red was conjugated onto the GA functionalized membrane surface by incubating the membrane in its solution (1 μg/mL) for 1 h. Finally, we gently rinsed the membrane with PBS and dried with N_2 spray to remove any low molecular weight and unreacted molecules from the surface.

2.3. Surface characterization of the membrane

We performed field emission scanning electron microscopy (FESEM) using FEI Magellan™ SEM, at an accelerating voltage of 5 kV with 160000x magnifications. We carried out atomic force microscopy (AFM) analysis with a Bruker Dimension Icon SPM in the resonance frequency range of 76-263 kHz under tapping mode. We conducted X-ray photoelectron spectroscopy (XPS) analysis using an AMICUS/ESCA 3400 KRATOS instrument equipped with an achromatic Al Kα X-ray source (1468.6 eV). The source was operated at a voltage of 10 kV and a current of 10 mA. The elemental narrow scan region was acquired with a step of 0.1 eV. We calibrated the obtained spectra using the reference C 1s at 284.8 eV. We deconvoluted the spectra using Gaussian and Lorentzian methods and we carried out background subtraction using the Tougaard method.

2.4. Fabrication of the organic electrochemical transistor (OECT)

We used a Parylene-C peel-off process to photo-lithographically fabricate the OECT, with a channel width of 100 μm and a channel length of 10 μm, on a glass substrate as described in Figure S2. We spin-coated a PEDOT:PSS dispersion containing EG, DBSA and GOPS to form the channels. After peeling off the sacrificial Parylene C layer, we annealed the devices at 140 °C for 1h and soaked in DI water overnight.

2.5. Preparation of amyloid-β monomer and aggregate solutions

We dissolved the protein in 10 mM PBS containing 0.5% ammonium hydroxide for a final concentration of 2.21 μM. We diluted this stock solution with PBS to the required concentrations in the range of 2.21 pM–221 nM. For the growth of the peptide (monomer) into an aggregate form, we incubated the solutions at 37 °C for 3 days and then stored them at −20 °C. For sensing experiments, we dropped 30 μL of the corresponding Aβ solution onto the CR functionalized membrane integrated transistors and allowed the reaction between the Aβ and CR to occur for 3 hours. We then rinsed the membrane integrated OECT with PBS and dried it with N_2 to remove any non-specific adsorption and non-binding molecules.

2.6. Characterization of the OECT and operation of the biosensor

We performed cyclic voltammetry (CV) and electrochemical impedance spectroscopy (EIS) measurements using a potentiostat (Metrohm Autolab) with a three-electrode configuration: the PEDOT:PSS channel of the OECT as the working electrode, a Pt mesh as the counter electrode and an Ag/AgCl as the reference electrode. The electrolyte solution was a PBS (0.01 M) solution containing 10 mM $K_3Fe(CN)_6$. We evaluated the OECT performance using a National Instruments-PXI digital multimeter controlled by a customized LabView program. We carried out the steady-state measurements of the OECTs by acquiring channel current (I_D) *vs*. drain voltage (V_D) at gate voltages (V_G) varying in between 0 and 0.6 V (step 0.05 V). We determined the sensor response from the transfer characteristics (I_D *vs*. V_G at a pre-set $V_D = -0.6$ V). We calculated the change in I_D at $V_G = 0$ V as the device was operated in solutions containing different Aβ concentrations. We calculated the current changes by subtracting the current at blank buffer and serum samples from the current at a specific concentration. We carried out all electrical measurements under ambient conditions and inside a grounded Faraday cage.

3. Results and discussion

3.1. Design of the functional membrane

The key element of this sensor is the nanostructured isoporous membrane (PS-*b*-P4VP) functionalized with Congo red (CR) molecules. This isoporous membrane is easily manufactured via self-assembly co-polymerization and non-solvent induced phase separation (Madhavan et al., 2014) (Figure S1) with an average nanopore size of about 50 nm (Fig. 1a). The immobilization of CR is a crucial step for selective and sensitive detection of Aβ aggregates. CR was selected as the recognition unit due to its stability in various media and strong affinity to Aβ aggregates (Nilsson, 2004; Pedersen and Heegaard, 2013). Fig. 1b displays the molecular structure of the polymer membrane and its functionalization route for immobilizing the CR. The functionalization of the nanostructured isoporous membrane was initiated by modification of the membrane with 3-aminopropyltriethoxysilane (APTES) to provide amino terminated groups on the surface. This was followed by reacting these groups with the bi-functional linker glutaraldehyde (GA). GA conjugates with the amino groups from the surface as well those of CR on the other end (Wustoni et al., 2015).

To verify the presence of CR on the membrane surface and analyze the surface after each modification step, we carried out XPS studies. The high-resolution of S2p, O1s and N1s spectra of the surface after APTES modification and upon CR immobilization reveal significant differences in the chemical composition of the membrane surfaces. We observe a characteristic peak on the S2p spectrum of the membrane only after the CR functionalization (Fig. 1c), i.e., a fingerprint of CR molecules that contain sulfur atoms on the $–SO_3$ functional groups in their structure. In the N1s spectra shown in Fig. 1d, the NH_2-functionalized membrane displays two deconvoluted peaks at 398.5 eV and 399.2 eV that belong to the nitrogen atoms in the terminal amino group of APTES and pyridine unit, respectively (Barber et al., 1973). Upon CR addition, we observe an additional small peak at 399.8 eV, which corresponds to an N═N bond of diazenyl functional group from the CR molecule (Camalli et al., 1990) (Table S1). Further evidence of the CR presence on the surface comes from the O1s spectra (Fig. 1e). For the NH_2-functionalized membrane, we deconvolute three peaks at 530.8 eV, 531.8 eV, and 533.3 eV, assigned for O-H, O-Si, O-C, bonds, respectively (Barr, 1983). Upon immobilization of the CR, new peaks at 535.1 eV and 536.7 eV appear, ascribed to the oxygen atoms in the $–SO_3$ groups of CR (Table S2). Our in-depth XPS characterization proves that the membrane surface has been successfully modified, first with APTES and then with CR. Importantly, after the modification with CR, the membrane maintains its porosity as shown in the SEM image in Figure S3.

3.2. OECT-based sensor for the detection of Aβ aggregates

To understand the operation mechanism of our sensor, it is crucial to understand how a depletion mode OECT works. In this device, we use a PEDOT:PSS film in the channel cast between source and drain contacts, and an Ag/AgCl pellet as the top gate electrode immersed into the measurement solution (Fig. 2a, left). In the absence of gate voltage (V_G), we record a high source-drain current (I_D) flowing in the channel due to the conducting nature of PEDOT:PSS. A positive voltage at the gate electrode (V_G) drifts the cations of the electrolyte into the channel, while anions move towards the gate electrode. I_D decreases with an increase in V_G (Fig. 2b). This is the result of the vertical drift and penetration of cations into the channel and the subsequent depletion of holes therein. The gain of the device (transconduntance) is maximized when V_G is ca. 0.1 V.

The configuration of our OECT biosensor involves the functionalized membrane placed on top of the PEDOT:PSS channel (Fig. 2a, middle). The device is then covered with a drop of electrolyte (PBS) and an Ag/AgCl top gate is immersed in it. The presence of the membrane does not interfere with the OECT operation: due to its porous nature, the membrane is permeable to electrolyte ions, thus allowing for efficient gating of the channel. However, when operating the device integrated with a membrane that is incubated in a solution containing Aβ aggregates (22.1 nM), we observe a substantial decrease in the channel current as well as the transconductance (Fig. 2b). This effect is more pronounced at low gate voltages. The latter is expected as there are fewer ions penetrating the channel at low bias. The respective output characteristics of the OECTs at each stage are shown in Figure S4.

The binding events affect also the transient characteristics of the device. For the transient response, we record the change in I_D upon application of a square-shaped pulse at the gate electrode ($V_G = 0.1$ V, 15 ms). The response times are then calculated from these transients shown in Fig. 2c, which gives the time for how fast the channel will be de-doped (doped) by injected (extracted) cations. The presence of the membrane on top of the channel decreases the current slightly with a negligible change in response time. On the other hand, upon incubation of the membrane with Aβ aggregates, the device switches ON and OFF more slowly, accompanied by a significant decrease in the current modulation. While the I_D in steady-state is proportional to the number of ions that can enter the film, the speed of the transistor is governed by the ionic flux (Jimison et al., 2012). Since the Aβ interactions with the CR is not electrochemically active and thus cannot directly induce an

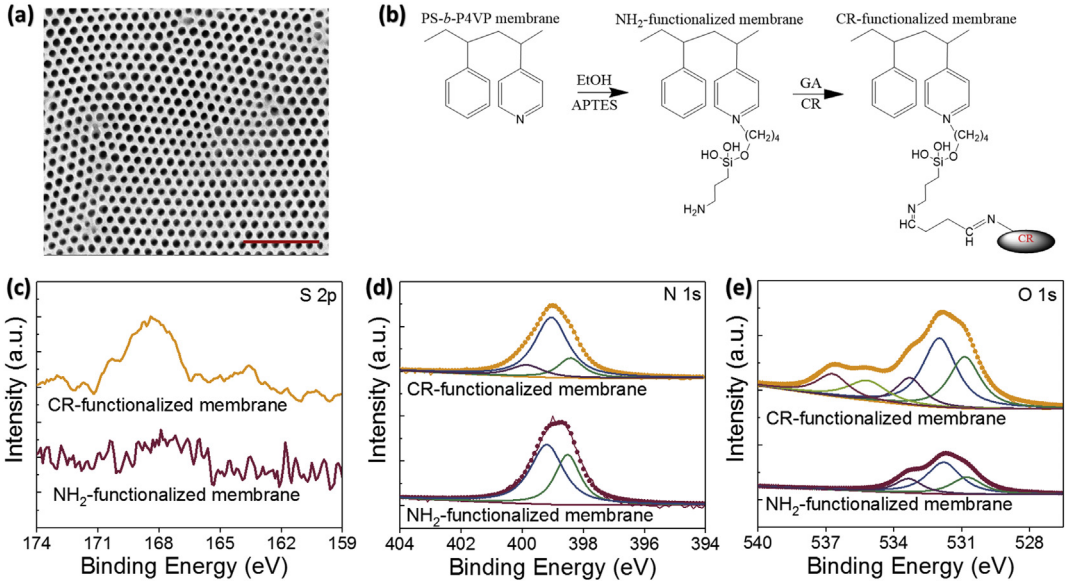

Fig. 1. Functionalization and characterization of the nanostructured, isoporous membrane. **(a)** SEM image of the PS-*b*-P4VP membrane. The scale bar is 500 nm. **(b)** Schematic representation of molecular functionalization of the PS-*b*-P4VP membrane with APTES to generate amino terminated groups on the surface and the subsequent immobilization of the CR via the GA linker. High-resolution S2p **(c)**, N1s **(d)**, and O1s **(e)** XPS spectra of the membrane after its modification with APTES (NH_2-functionalized membrane) and CR (CR-functionalized membrane).

electrical signal, it is clear that the device characteristics are modulated by the permeability of the membrane.

The changes in the AFM images and XPS spectra of the membrane upon interactions with Aβ aggregates evidence that CR units capture the protein aggregates which then adsorb on the membrane surface (Figure S5; Table S1-S2). We designed the membrane such that its pore size (i.e., ca. 50 nm) is smaller than that of Aβ aggregates (e.g. protofibrils) (Ochiishi et al., 2016; Wolff et al., 2017). The adsorbed protein aggregates thus clog the membrane pores and block partially the transport of ions from the electrolyte into the channel (Fig. 2a, right). Consequently, we measure a decrease in the total number of cations that can enter the channel and, in their flux (i.e., lower transconductance and slower response time).

In order to validate our hypothesis, we further performed cyclic voltammetry (CV) and electrochemical impedance spectroscopy (EIS) measurements (Figure S6). We studied the same OECT channel before and after integration with the membrane and after Aβ incubation in an electrolyte containing the redox active molecule $K_3Fe(CN)_6$ to evaluate the kinetic barrier at the channel/electrolyte interface (Cardoso et al., 2016). The results show that after incubation with Aβ aggregates, the peak currents decrease drastically, indicating that Fe^{3+} transport towards the channel is hindered. In addition, the channel capacitance decreases accompanied with an increase in charge transfer and electrolyte resistance due to a drop in the ion diffusion ability.

A feature of this device configuration is its prolonged shelf life and operational stability. This is because we compartmentalize the sensing event. The binding events happen in the functionalized membrane that can be replenished when needed, while the electronic device

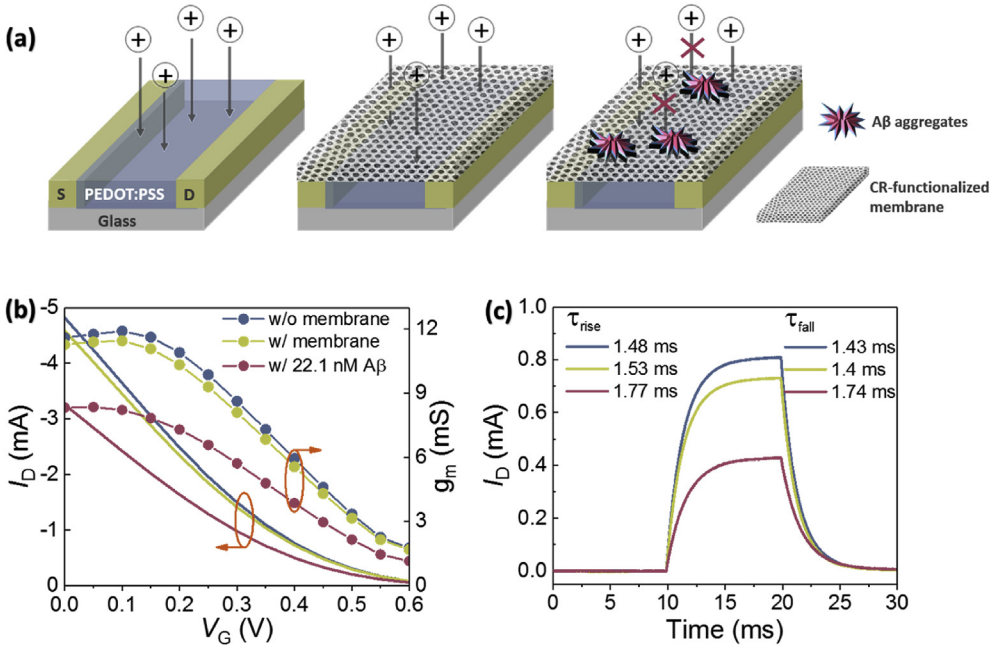

Fig. 2. The OECT biosensor configuration and characteristics. **(a)** The CR-functionalized membrane is placed between the channel and the electrolyte solution (middle). Cation drift into the PEDOT:PSS channel is impaired because of the Aβ aggregates adsorbed on the membrane (right). The transfer characteristics **(b)** and transient characteristics **(c)** of an OECT before and after integration with the membrane as well as upon incubation of the membrane with Aβ aggregate solution (22.1 nM, PBS). The channel has a width of 10 µm and length of 100 µm. For the transients, V_G = 0.1 V with a length of 15 ms.

underneath is kept “pristine” so as to maintain its function for further use. As such, the device is expected to have significantly longer shelf life than other sensors that rely on biofunctionalized electronic elements. As shown in Figure S7a, the current flowing in the PEDOT:PSS channel is identical before and after the integration with the membrane, as well as after the device has been utilized several times for Aβ sensing. The same OECT can then be integrated with fresh membranes for new measurements (Figure S7b). This configuration is also cost effective because for this particular sensor, the fabrication of the OECT chip requires more sophisticated procedures than that of the membrane. Moreover, the membrane-integrated OECT has operational stability similar to a bare OECT, i.e., the device shows stable drain current output when stressed with 5 s long, continuous square-shaped pulses at the gate electrode for more than 15 minutes (Figure S7c-d).

3.3. Sensitivity of the biosensor

In the experiments above, we tested the device response only to a particular Aβ aggregate concentration. We also do not know whether the interactions of Aβ aggregates is specific to CR units as envisaged or whether the Aβ aggregates would nonspecifically adsorb on a CR-free membrane surface. Fig. 3 a and b show the steady-state characteristics of an OECT channel integrated with a CR-functionalized membrane, and with a bare PS-*b*-P4VP membrane incubated with Aβ solutions of a broad range of concentrations, respectively. The transfer curve of the functionalized membrane integrated OECT shows that a continuous decrease in the drain current with an increase in the Aβ aggregate concentration (Fig. 3a). The CR-free, bare membrane, on the other hand, has no specific interactions with Aβ aggregates, leading to a device response independent of protein concentration (Fig. 3b).

Fig. 3c demonstrates the calibration curve of our biosensor (the current change *vs* the logarithm of Aβ concentration), showing a linear response towards the Aβ aggregates in the range of 2.21 pM–221 nM. The slope of this linear curve is 216 μA/dec. The sensitivity of the device outperforms the previously reported electrochemical systems thanks to the high transconductance endowed by the OECT circuitry, as summarized in Table S3. To rule out the possibility of the CR-functionalized membrane also interacting with the Aβ monomers, we monitored the device response to a broad range of peptide concentrations. The negligible change in channel conductance with the peptide confirms the selectivity of the sensor to the aggregate form of the protein. Accordingly, when we incubate the membrane with Aβ monomers, its surface morphology does not change (Figure S8). CR molecules capture only the aggregate form of the protein that contains cross-β structure conformation whereas they do not bind to the peptide with α-helix-rich structure (Wu et al., 2007, 2012). Likewise, the device is not sensitive to Aβ aggregates if the membrane does not carry CR units. These results demonstrate the key role of the CR units to capture the Aβ aggregates and identify the physical state of the proteins.

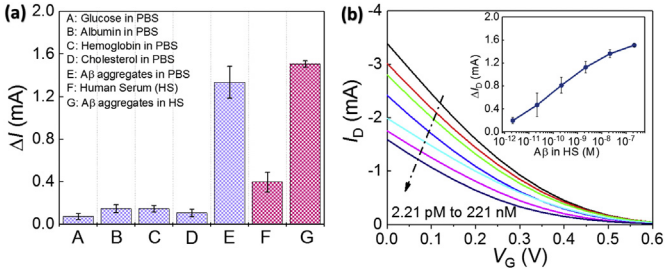

Fig. 4. Specificity and selectivity of the OECT biosensor in complex media. **(a)** The OECT response to Aβ aggregates and potential interferents in PBS as well as to Aβ aggregates in a human serum sample (glucose: 10 mM, albumin: 3.5 mg/mL, cholesterol: 0.1 mg/mL; hemoglobin: 0.02 mg/mL, Aβ: 22.1 nM). The blue and red bars represent PBS and serum samples, respectively, as the medium. **(b)** Transfer curves of an OECT biosensor for *in vitro* analysis of Aβ aggregates which were spiked in the human serum sample, and the corresponding calibration plot (inset). For (a) and the inset of (b), error bars represent the SD of the response collected from three and eight identical channels, respectively, operated at V_D of −0.6 V and V_G of 0 V. (For interpretation of the references to colour in this figure legend, the reader is referred to the Web version of this article.)

3.4. Operation in complex media

Aβ aggregates are reported to be released into blood plasma (De la Escosura-Muñiz et al., 2015). The detection of Aβ aggregates in human serum samples could thus offer a portable, non-invasive and low-cost option for *in vitro* monitoring of AD. To test the performance of our sensor in complex media, we emulated complex media conditions using commonly interfering species such as glucose, hemoglobin, cholesterol and human serum albumin proteins, and evaluated the sensor performance therein as well as in human blood serum (HS). Fig. 4a shows a comparison of the OECT response to these interferents in PBS, which is insignificant compared to the response to Aβ aggregates. While the HS, which contains a large number of biomolecules, generates a background current, this does not hinder the device sensitivity to Aβ aggregates. Similar to the dose-dependent response of the device recorded in PBS (Fig. 3a), the OECT current decreases linearly with an increase in the concentration of Aβ aggregates in HS (Fig. 4b). The device is also not responsive to molecules which can clog the membrane pores because of their size, further evidencing that the specific interactions of Aβ aggregates with CR is essential for their detection (Figure S9).

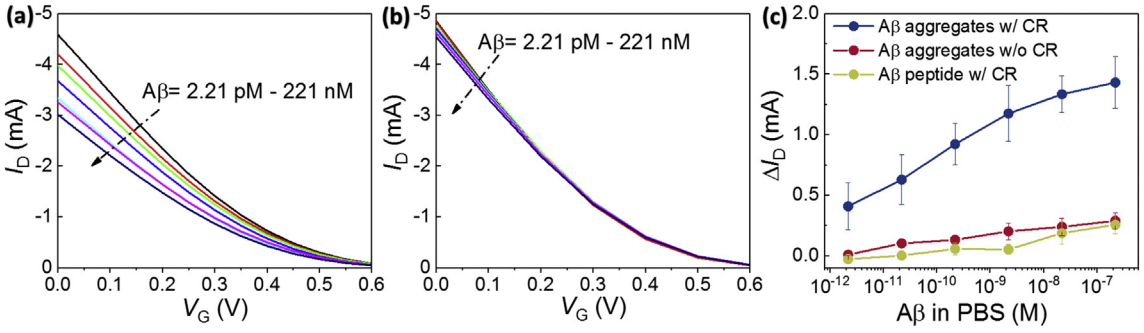

Fig. 3. Dose curves and the specificity of the sensor towards Aβ aggregates. Transfer characteristics of the OECT channel integrated with a CR-functionalized membrane **(a)** and a bare PS-*b*-P4VP membrane **(b)**. Each membrane was exposed to Aβ aggregate solutions of varying concentrations (from 2.21 pM to 221 nM) **(c)** The current response of OECT biosensor (i.e., OECT integrated with CR-functionalized membrane) to Aβ aggregates. The response of the device to Aβ peptide is shown by the yellow curve. Error bars represent the SD from measurements from at least three channels operated at V_D of −0.6 V and V_G of 0 V. (For interpretation of the references to colour in this figure legend, the reader is referred to the Web version of this article.)

4. Conclusion

In this work, we develop a bio-functional, nanostructured, isoporous membrane integrated OECT for the rapid and sensitive detection of Aβ protein aggregates. The Congo red units anchored on the membrane surface enables selective capture of Aβ aggregates. The membrane is placed on top of the OECT channel. As the aggregates are larger than the size of membrane pores, once they are captured by the membrane, they block the drift of electrolyte cations into the channel during the OECT operation. The drain current is thus modulated in correlation with the amount of aggregates adsorbed from the electrolyte. We, therefore, combine three concepts to build this state-of-the-art sensor: 1) biomolecular interactions of Congo red only with Aβ aggregates; 2) the size-selective blockage of the ion pathways; 3) high sensitivity of the OECT channel to electrolyte cations. The use of a CR-functionalized membrane as the recognition unit has several advantages: the sensor has long term stability, ease of use, and low-cost compared to antibodies or enzymes. Thanks to the isoporosity and selectivity of the membrane, we show in particular that neither Aβ monomers nor physically adsorbed Aβ aggregates influence ion penetration, thus rendering the sensor highly specific to CR-captured Aβ aggregates. The label-free protein sensor linearly detects the Aβ aggregates from 2.21 pM to 221 nM in the buffer and human serum sample, in the range of standard physiological concentrations. Considering the selectivity and sensitivity of this approach, our work paves the way for advanced electronic platforms for early diagnosis of AD. In addition, this work can inspire the use of porous membranes functionalized with various biorecognition units and their integration with miniaturized, high transconductance transistors.

Declaration of interest

A patent application about the device architecture and methods of use thereof was filed by S.W. and S.I., pending with the application number of 62882481. The remaining authors declare no competing interests.

CRediT authorship contribution statement

Shofarul Wustoni: Validation, Investigation, Writing - original draft. **Shaofei Wang:** Resources, Investigation, Validation. **Juan R. Alvarez:** Resources, Investigation. **Tania C. Hidalgo:** Resources. **Suzana P. Nunes:** Funding acquisition, Writing - review & editing. **Sahika Inal:** Conceptualization, Writing - review & editing, Supervision, Funding acquisition.

Acknowledgments

S. W. and S. I. gratefully acknowledge financial support from the KAUST Office of Sponsored Research (OSR) under Award CRF-2019-SENSORS-2719.

Appendix A. Supplementary data

Supplementary data to this article can be found online at https://doi.org/10.1016/j.bios.2019.111561.

References

Alzheimer's Diseases International, 2018. World Alzheimer Report. . https://www.alz.co.uk/research/WorldAlzheimerReport2018.pdf?2 accessed on 13 March 2019.
Barber, M., Connor, J.A., Guest, M.F., Hillier, I.H., Schwarz, M., Stacey, M., 1973. J. Chem. Soc., Faraday Trans. 2 (69), 551–558.
Barr, T.L., 1983. Appl. Surf. Sci. 15 (1), 1–35.
Camalli, M., Caruso, F., Mattogno, G., Rivarola, E., 1990. Inorg. Chim. Acta 170 (2), 225–231.
Cardoso, A.R., Moreira, F.T.C., Fernandes, R., Sales, M.G.F., 2016. Biosens. Bioelectron. 80, 621–630.
Dalal, V., Bhattacharya, M., Narang, D., Sharma, P.K., Mukhopadhyay, S., 2012. J. Phys. Chem. Lett. 3 (13), 1783–1787.
De la Escosura-Muñiz, A., Plichta, Z., Horák, D., Merkoçi, A., 2015. Biosens. Bioelectron. 67, 162–169.
Fu, Y., Wang, N., Yang, A., Law, H.K.-w., Li, L., Yan, F., 2017. Adv. Mater. 29 (41), 1703787.
Ghittorelli, M., Lingstedt, L., Romele, P., Crăciun, N.I., Kovács-Vajna, Z.M., Blom, P.W.M., Torricelli, F., 2018. Nat. Commun. 9 (1), 1441.
Gualandi, I., Tonelli, D., Mariani, F., Scavetta, E., Marzocchi, M., Fraboni, B., 2016. Sci. Rep. 6, 35419.
Hardy, J., Selkoe, D.J., 2002. Science 297, 353–356.
He, R.-X., Zhang, M., Tan, F., Leung, P.H.M., Zhao, X.-Z., Chan, H.L.W., Yang, M., Yan, F., 2012. J. Mater. Chem. 22 (41), 22072–22076.
Jimison, L.H., Tria, S.A., Khodagholy, D., Gurfinkel, M., Lanzarini, E., Hama, A., Malliaras, G.G., Owens, R.M., 2012. Adv. Mater. 24 (44), 5919–5923.
Kim, D.-J., Lee, N.-E., Park, J.-S., Park, I.-J., Kim, J.-G., Cho, H.J., 2010. Biosens. Bioelectron. 25 (11), 2477–2482.
LaFerla, F.M., Green, K.N., Oddo, S., 2007. Nat. Rev. Neurosci. 8, 499–509.
Liu, L., He, Q., Zhao, F., Xia, N., Liu, H., Li, S., Liu, R., Zhang, H., 2014. Biosens. Bioelectron. 51, 208–212.
Lopes, P., Xu, M., Zhang, M., Zhou, T., Yang, Y., Wang, C., Ferapontova, E.E., 2014. Nanoscale 6 (14), 7853–7857.
Macchia, E., Romele, P., Manoli, K., Ghittorelli, M., Magliulo, M., Kovacs-Vajna, Z.M., Torricelli, F., Torsi, L., 2018. Flex. Print. Electron. 3, 034002.
Madhavan, P., Hong, P., Sougrat, R., Nunes, S.P., 2014. Appl. Mater. Interfaces 6, 18497–18501.
Mariani, F., Gualandi, I., Tessarolo, M., Fraboni, B., Scavetta, E., 2018. ACS Appl. Mater. Interfaces 10, 22474–22484.
Nilsson, M.R., 2004. Methods 34, 151–160.
Ochiishi, T., Itakura, A., Liu, L., Akatsu, H., Kohno, H., Nishimura, M., Yoshimune, K., 2016. Genes Cells 21 (2), 200–211.
Pappa, A.M., Ohayon, D., Giovannitti, A., Maria, I.P., Savva, A., Uguz, I., Rivnay, J., McCulloch, I., Owens, R.M., Inal, S., 2018. Sci. Adv. 4 (6), eaat0911.
Parlak, O., Keene, S.T., Marais, A., Curto, V.F., Salleo, A., 2018. Sci. Adv. 4 (7), eaar2904.
Pedersen, J.T., Heegaard, N.H.H., 2013. Anal. Chem. 85, 4215–4227.
Pinotsi, D., Buell, A.K., Dobson, C.M., Kaminski Schierle, G.S., Kaminski, C.F.A., 2013. Chembiochem 14 (7), 846–850.
Rivnay, J., Inal, S., Salleo, A., Owens, R.M., Berggren, M., Malliaras, G.G., 2018. Nat. Rev. Mater. 3, 17086.
Schöneich, C., Pogocki, D., Hug, G.L., Bobrowski, K., 2003. J. Am. Chem. Soc. 125, 13700–13713.
Sessolo, M., Rivnay, J., Bandiello, E., Malliaras, G.G., Bolink, H.J., 2014. Adv. Mater. 26 (28), 4803–4807.
Suprun, E.V., Khmeleva, S.A., Radko, S.P., Kozin, S.A., Archakov, A.I., Shumyantseva, V.V., 2016. Electrochem. Commun. 65, 53–56.
Vas, C.J., Rajkumar, S., Tanyakitpisal, P., Chandra, V., 2001. Alzheimer's Disease: the Brain Killer. World Health Organization.
Vestergaard, M.d., Kerman, K., Saito, M., Nagatani, N., Takamura, Y., Tamiya, E.A., 2005. J. Am. Chem. Soc. 127 (34), 11892–11893.
Walsh, D.M., Klyubin, I., Fadeeva, J.V., Cullen, W.K., Anwyl, R., Wolfe, M.S., Rowan, M.J., Selkoe, D.J., 2002. Nature 416, 535–539.
Wang, N., Yang, A., Fu, Y., Li, Y., Yan, F., 2019. Acc. Chem. Res. 52 (2), 277–287.
Wolff, M., Zhang-Haagen, B., Decker, C., Barz, B., Schneider, M., Biehl, R., Radulescu, A., Strodel, B., Willbold, D., Nagel-Steger, L., 2017. Sci. Rep. 7 (1), 2493.
Wu, C., Scott, J., Shea, J.-E., 2012. Biophys. J. 103 (3), 550–557.
Wu, C., Wang, Z., Lei, H., Zhang, W., Duan, Y., 2007. J. Am. Chem. Soc. 129 (5), 1225–1232.
Wustoni, S., Hideshima, S., Kuroiwa, S., Nakanishi, T., Hashimoto, M., Mori, Y., Osaka, T., 2015. Biosens. Bioelectron. 67, 256–262.
Wustoni, S., Savva, A., Sun, R., Bihar, E., Inal, S., 2019. Adv. Mater. Interfaces 6, 1800928.